Measurement of Defibrillator Surface Potentials for Simulation Verification

Jess D Tate[1,2], Jeroen G Stinstra[2], Thomas A Pilcher[3], Rob S MacLeod[1,2]

[1]Department of Bioengineering, University of Utah, Salt Lake City, Utah, USA
[2]Scientific Computing and Imaging Institute, University of Utah, Salt Lake City, Utah, USA
[3]Primary Children's Medical Center, Salt Lake City, Utah, USA

Abstract

Despite the growing use of implantable cardioverter defibrillators (ICDs) in adults and children, there has been little progress in optimizing device and electrode placement. To facilitate effective placement of ICDs, especially in pediatric cases, we have developed a predictive model that evaluates the efficacy of a delivered shock. Most recently, we have also developed an experimental validation approach based on measurements from clinical cases. The approach involves obtaining body surface potential maps of ICD discharges during implantation surgery and comparing these measured potentials with simulated surface potentials to determine simulation accuracy. Comparison of the simulated and measured potentials yielded very similar patterns and a typical correlation greater than 0.9, suggesting that the predictive simulation generates realistic potential values. Ongoing sensitivity studies will determine the robustness of the results and pave the way for use of this approach for assisting optimization of ICD use.

1. Introduction

Implantable Cardioverter Defibrillators (ICDs) are becoming more commonly used to prevent sudden death due to cardiac arrhythmias with over 114,000 implantations in 2006 alone [1]. Though these devices save many lives each year, ICDs have yet to be designed or optimized for a growing population of pediatric patients that are receiving treatment from them [2]. Because of geometry constraints and the high occurrence of device replacement, many pediatric cardiologists have used difference ICD placement strategies that are meant to increase the safety of the patient and facilitate replacement the device [3]. There is also risk of using excessive energy because such shocks have been shown to disrupt Ca^{++} dynamics in the myocardium [4]. Both the need for new configurations and the risk of over shock provide motivation to determine optimal ICD placements to provide effective defibrillation treatment with the least amount of energy possible for pediatrics patients.

We have developed a patient specific computational simulation that predicts the energy required to defibrillate the heart, for a given position of the ICD [5]. This simulation calculates that potential field throughout the torso based on the patient's tissue geometry obtained from MRI or CT scans and the ICD location. From the resulting electric field in the myocardium, we predict defibrillation threshold. Initial studies show that the simulation is accurate in predicting the defibrillation threshold [5], but a validation of the calculated potential field in humans is desired to provide deeper insight in the ability of the model to predict the behavior of ICDs in real patients.

In this paper, we adapted a limited lead selection and body surface map estimation algorithm developed by Lux *et al.* [6] to ICD potential distributions to allow comparison of simulated and recorded surface potentials. Recording of ICD surface potentials requires the instance of known ICD discharges, limiting the opportunity for measurement to the implantation procedure when the device is tested in each patient, though the environment significantly limits the space on the body surface for recording. THe spatial limitations of the testing environment excludes the use of many potential mapping schemes, in which many regularly spaced electrodes are placed on the torso surface. However, with body surface map estimation one is able to obtain a full potential map from a small number of electrodes, providing statistical information of the potential distributions are known [6]. Using simulated surface potential maps to generate the statistical information, we were able to estimate the full potential maps of ICD discharges from 32 electrode recordings with high accuracy.

2. Methods

The application of the limited lead selection and body surface estimation algorithm was performed with a database of simulated potential maps. The application of the algorithm, as illustrated in Figure 1, involved predicting a subset of lead locations that provide accurate reconstruction, determining statistical correlation between the lead subset and the full potential map, applying the transformation determined by the statistical correlation to gen-

erate estimated potential maps, and evaluating the estimated potential maps for accuracy.

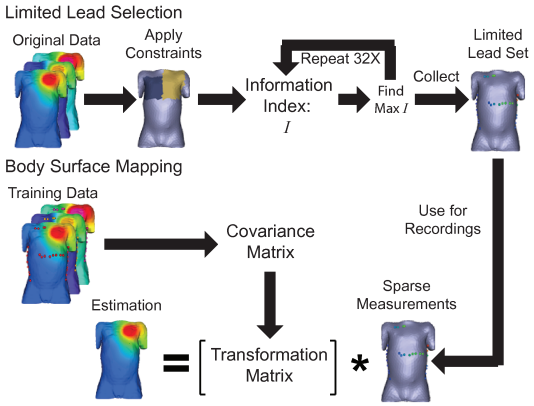

Figure 1. Application of the limited lead selection and the body surface estimation algorithm used to measure the ICD surface potential maps.

2.1. Limited lead selection

In order to generate full torso potential maps of the ICD discharge from a small subset of lead locations the best subset was found. The limited lead selection predicts the leads which add the most specificity to potential map estimation by calculating the locations most likely to provide unique information to the potential map, or information index. The information index is calculated based on the standard deviation and the covariance of the potential maps available in the database used to train the algorithm. By calculating the information index for each location, choosing the highest index, and recalculating the index after that location is removed from consideration, the limited leads were calculated one by one until the required number of leads were found (Figure 1). Constraints that reflect the spatial limitations of the implantation procedure were applied to this algorithm to yield locations that were used in the body surface estimation algorithm [6].

2.2. Training for estimation

With the optimal limited lead set identified, the body surface potential mapping algorithm must be trained to the statistical variation of the ICD potential distributions [6]. The training is based on a dataset of simulated ICD potential maps from eight patient geometries with 37 differing conductivity schemes for a total of 296 potential maps. The conductivities were varied to provide statistical variance and numerical stability to the training algorithm. The training database allowed for accurate estimation on a variety of geometries.

The training of the body surface estimation algorithm involves finding the parameters to relate subsets of the surface potential vector P; the algorithm correlates the limited lead potentials (P_1) and the potentials of the rest of the estimated potential map (P_2), to satisfy the expression:

$$\hat{P}_2 = \bar{P}_2 + T \cdot (P_1 - \bar{P}_1). \quad (1)$$

where $\hat{P}_2$ is the estimated P_2, T is a transformation matrix, and $\bar{P}_1$ and $\bar{P}_2$ are the subsets of the vector that expresses the mean of each location $\bar{P}$. The matrix T was calculated from the covariance matrix K:

$$T = K_{12}^T K_{11}^{-1}. \quad (2)$$

where K_{12} and K_{11} are subsets of K relating to P_1 and P_2 so that

$$K = \begin{bmatrix} K_{11}K_{12} \\ K_{21}K_{22} \end{bmatrix}. \quad (3)$$

With the transformation matrix T calculated in this way, body surface estimation was performed on simulated and measured potentials [6].

2.3. Estimating the ICD shock potentials

The estimation of the ICD potential distribution involves obtaining potentials from the limited lead set (P_1) and estimating the rest of the potential map ($\hat{P}_2$) as expressed in Eq. 1. As indicated, the training of the algorithm yielded the mean vectors ($\bar{P}_1$ and $\bar{P}_2$) and the transformation matrix T and allowed for the computation of the $\hat{P}_2$ with the appropriate P_1 [6].

The body surface estimation was calculated with both simulated and measured data. Estimation of simulated surface potentials provides a direct method of analysis of this application of the algorithm, and was performed on a separated database of 160 ICD surface potentials generated from the same eight geometries and 20 conductivity schemes which were difference from the previous schemes used. These potential maps were each sampled at the limited lead set locations to provide the vector P_1, and the potential map was estimated as in Eq. 1.

Estimation of the potential maps based on recorded surface potentials requires some addition considerations, including the acquisition of the surface recordings and relating those time dependent recordings to the single instance simulation. The acquisition of the surface recordings was performed on patients scheduled for ICD implantation. An array of 32 recording electrodes (plus one reference and one ground) were attached to the patient in a configuration similar to the calculated limited lead set at the beginning of the implantation procedure. During the device testing,

surface potentials were recorded using a 32 channel, 16 bit acquisition system with an attenuator (signal reduction by 10,000) at a sampling rate of 1 or 4 kHz. The temporal recordings were then correlated to the single instant simulation by sampling the 32 channels at the peak of the first pulse and used Eq. 1 as P_1.

Evaluation of the body surface estimation was performed on reconstructions from simulated and measured data by correlation coefficient, relative error, and the RMS error. The estimations based on simulated potentials were evaluated with respect to the potential map from which the subset was sampled and estimations based on surface recording were evaluated against the corresponding patient specific simulation generated from the MRI scan and the ICD placement.

3. Results

Evaluation of the body surface estimation from the simulated surface potentials demonstrated high levels of accuracy. The average overall metrics of the estimation on the dataset include a correlation of 0.99984 $\pm$ 3e-5, relative error of 0.033 $\pm$ 0.005 %, and RMS error of 2.1 $\pm$ 0.1 V. Figure 2 illustrates the typical absolute error by location (average max error of 16.2 $\pm$ 1.0 V) based on a 500 V shock. As indicated, the areas of most error are located on the left shoulder inferior to the clavicle. This is the where the device was located in the simulations and in each of the cases recorded. Though the error is substantially higher in this area than the rest of the torso, the max error is low compared to the magnitude of the shock.

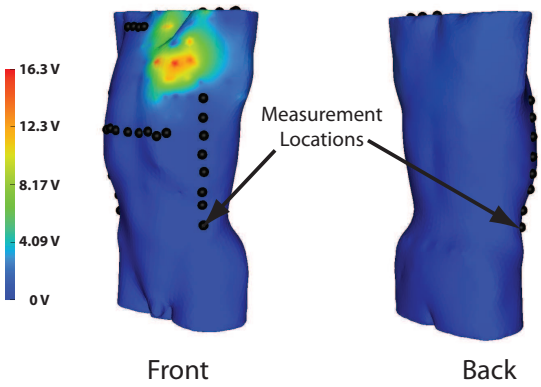

Figure 2. Typical absolute error between actual and reconstructed potentials by location from a shock with 500 V magnitude. Black points indicate the limited lead set used in the reconstruction.

Estimation of body surface potentials from ICD potential recordings also demonstrated strong similarities. As shown in Figure 3, the estimated potential maps have qualitatively similar profiles to the corresponding simulated maps. Similarly, the evaluation of the reconstruction compared to the patient specific simulation revealed quantitative similarities with an average correlation of 0.977 $\pm$ 0.002, relative error of 7 $\pm$ 1 %, and RMS error of 22 $\pm$ 3 V. Figure 3 reveals the areas of high area to be near the device location.

4. Discussion and conclusions

The data shown indicate that the body surface estimation algorithm applied to recorded ICD surface potentials can generate accurate potential maps. The estimation of simulated surface potential produced highly accurate potential maps (Figure 2), demonstrating the possibility of using the estimation algorithm on ICD potentials and generating a level of accuracy that can be used in the validation of the simulation in humans. The proof of concept of the algorithm is further supported by the potential map estimations generated from ICD surface recordings. The qualitative and quantitative comparisons of these reconstructions (Figure 3) provides a level of validation that has not been possible before, allowing for high resolution evaluation between simulation and measurements.

Though we have demonstrated estimations of ICD potential maps that are similar to simulated results, the compared potential maps also indicate deficiencies in the simulation that need to be corrected. When comparing the potential maps point by point, there is often higher error expressed than when comparing the potential maps together. These errors could not be rectified by changing only a single conductivity parameter, indicating an overlooked complexity in the current model. Such complexities that might effect the surface potentials include anisotropy of the cardiac tissue and including more or different tissue types. Future work on the simulations will include exploration of each of these complexities. Future validation work includes the evaluation of the ICD discharge in a volume based on phantoms and isolated hearts. This evaluation may provide insight on volumetric and time dependent properties of the ICD discharge.

Acknowledgements

The research presented in this paper was made possible with help from Philip Erchler and Bruce Steadman from Cardiovascular Research and Training Institute, Elizabeth Saarel from Primary Children's Medical Center, John Triedman from Children's Hospital Boston, Matthew Jolley from Stanford University, and Ahrash Poursaid from the University of Utah.

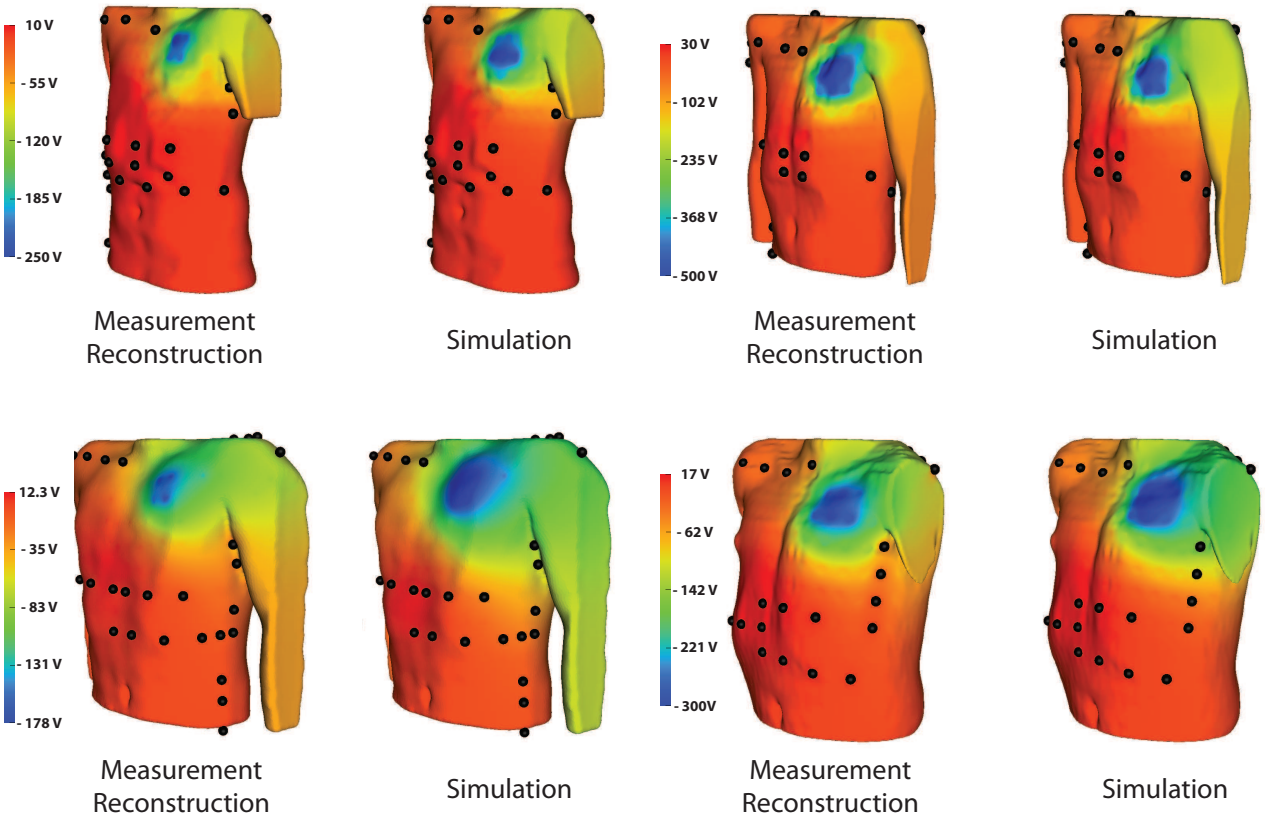

Figure 3. Surface potential comparison between the reconstruction obtained from surface recordings and the simulation. Black points indicate measurement locations for the subset used in the reconstructions.

References

[1] Lloyd-Jones D, Adams RJ, Brown TM, Carnethon M, Dai S, De Simone G, Ferguson TB, Ford E, Furie K, Gillespie C, Go A, Greenlund K, Haase N, Hailpern S, Ho PM, Howard V, Kissela B, Kittner S, Lackland D, Lisabeth L, Marelli A, McDermott MM, Meigs J, Mozaffarian D, Mussolino M, Nichol G, Roger VL, Rosamond W, Sacco R, Sorlie P, Stafford R, Thom T, Wasserthiel-Smoller S, Wong ND, Wylie-Rosett J, on behalf of the American Heart Association Statistics Committee, Subcommittee SS. Heart disease and stroke statistics–2010 update: A report from the american heart association. Circulation 2010;121(7):e46–215. URL `http://circ.ahajournals.org`.

[2] Kugler JD, Erickson CC. Nontransvenous implantable cardioverter defibrillator systems: not just for small pediatric patients. J Cardiovasc Electrophysiol January 2006;17(1):47. ID: 17; PUBM: Print; JID: 9010756; ppublish 1045-3873 Journal.

[3] Cannon B, Friedman R, Fenrich A, Fraser C, McKenzie E, Kertesz N. Innovative techniques for placement of implantable cardioverter-defibrillator leads in patients with limited venous access to the heart. PACE 2006;29:181–187.

[4] Ristagno G, Wang T, Tang W, Sun S, Castillo C, Weil MH. High-energy defibrillation impairs myocyte contractility and intracellular calcium dynamics. Critical Care Medicine 2008;36(11)(SupplNovember):S422–S427.

[5] Jolley M, Stinstra J, Pieper S, MacLeod R, Brooks DH, Cecchin F, Triedman JK. A computer modeling tool for comparing novel ICD electrode orientations in children and adults. Heart Rythm J 2008;5(No 4, April 2008):565–572.

[6] Lux RL, Smith CR, Wyatt RF, Abildskov JA. Limited lead selection for estimation of body surface potential maps in electocardiography. IEEE Trans Biomed Eng 1978;BME-25, No. 3(May 1978):270–276.

Address for correspondence:

Jess Tate
Scientific Computing and Imaging Institute
WEB, 72 South Campus Drive, Rm 3750
Salt Lake City, UT 84112
jess@sci.utah.edu